The solvent-free selective hydrogenation of nitrobenzene to aniline: an unexpected catalytic activity of ultrafine Pt nanoparticles deposited on carbon nanotubes

Zhenyu Sun, Yanfei Zhao, Yun Xie, Ranting Tao, Hongye Zhang, Changliang Huang and Zhimin Liu*

Received 3rd February 2010, Accepted 31st March 2010
First published as an Advance Article on the web 11th May 2010
DOI: 10.1039/c002391d

In this work, we developed a facile and efficient route to deposit ultrafine Pt particles onto multi-walled carbon nanotubes (MWNTs) with the aid of tip sonication. The loading of Pt on the MWNTs could attain the very high level of 50 wt% and the size of the Pt particles could be controllably tuned in the range 1.9–3.5 nm with narrow size distributions. The resultant nanocomposites were applied to catalyze the hydrogenation of nitrobenzene under solvent-free conditions. It was demonstrated that the Pt/MWNT catalysts showed excellent activity with a high turnover frequency (*e.g.*, 69 900 h^{-1}) as well as superior selectivity to aniline (*e.g.*, >99%) in this reaction.

Introduction

About 85% of global aniline, a valuable intermediate for polyurethanes, dyes, pharmaceuticals, explosives, *etc.*, is produced from the catalytic hydrogenation of nitrobenzene (NB).[1] Commercially, NB hydrogenation is usually performed in the vapor phase at 473 K over copper-based catalysts.[2] Alternatively, the reaction can also be conducted in the liquid phase over Ni catalysts at 353–393 K.[3] A number of groups have also reported liquid-phase hydrogenation over noble metals (Pd, Pt, Ru) supported on various substrates under mild conditions.[4–5] Nevertheless, most reaction processes suffer from one or more disadvantages, such as using organic solvents that are associated with serious toxicity issues, poor selectivity and thus the formation of undesirable by-products, including nitrosobenzene (NSB), *N*-phenylhydroxylamine (PHA), azoxybenzene (AOB), azobenzene (AB) and hydrazobenzene (HAB). In such scenarios, it is desirable to develop greener and rapid processes for the selective hydrogenation of NB to produce aniline, especially under mild and solvent-free conditions. To achieve this goal, the design of catalysts suitable for this reaction is key. To date, Pt nanoparticles (NPs) decorated on an active carbon support (Pt/C) have been identified as the best catalyst for NB hydrogenation; however, the reaction rate and selectivity to aniline using this catalyst are lower than expected in both solvent and solvent-free conditions.[6] Therefore, it should be very interesting to explore highly active and selective catalysts for application in the greener hydrogenation of NB under solvent-free conditions.

The intriguing structural perfection and superlative physical properties of carbon nanotubes (CNTs) make them a potentially good candidate for a wide range of novel applications. In particular, CNTs are considered to be attractive catalyst supports owing to their remarkable structure-dependent properties, such as high tensile strength, large surface area, and high electric and thermal conductivity.[7–13] Moreover, CNTs as supports are characterized by excellent resistance against corrosion compared to carbon black[14,15] and allow better contact between the reactant and the catalytic component than porous carbons. CNT-supported metals have been widely investigated and have shown promising applications in catalysis.[14,15]

Herein, we investigate the catalytic performance of Pt/MWNT for NB hydrogenation under solvent-free conditions. Varying the parameters, including the Pt loading in Pt/MWNT, the H_2 pressure and the reaction temperature, was studied with respect to the reaction. A possible reaction pathway is also discussed. The Pt/MWNT catalysts were obtained by the use of a very simple sonication process, and were characterized in detail by transmission electron microscopy (TEM), high-resolution TEM (HRTEM) and X-ray photoelectron spectroscopy (XPS).

Results and discussion

In this work, we first developed a very simple and efficient process to deposit ultrafine Pt particles onto MWNTs *via* tip sonication. The pronounced features of this method involve the following aspects: (1) the size of the Pt NPs can be tuned from 1.9 to 3.5 nm with very narrow size distributions and the Pt loading can reach a very high level (*e.g.*, 50 wt%), (2) no harsh pre-treatments or covalent functionalization of the CNTs is required, which can avoid unduly disrupting the π system and degrading the electronic properties of the CNTs, (3) no stabilizer (*i.e.*, organic species, surfactants) for the Pt NPs is required, which can preclude the problem where the stabilizer molecules occupy the active sites of the catalyst. Moreover, this strategy can be generally applied to immobilize other noble metals (Ru, Pt/Ru, Au, Pd, AuPd, Ag) onto MWNT supports, as well as Pt NPs loaded onto single-walled CNTs, and hence provide a versatile way for synthesizing supported nanocatalysts.

Institute of Chemistry, Chinese Academy of Sciences, Beijing, 100190, P. R. China. E-mail: liuzm@iccas.ac.cn

A TEM observation was carried out to gather information about the microstructure of the resultant Pt/MWNT catalysts. Fig. 1a–e shows typical TEM images, together with Pt particle size distribution histograms, for the catalysts with Pt loadings varying from 10 to 72.1 wt%. The histogram of the Pt particle size (diameter) distribution was extracted by directly measuring 100 particles from the TEM view, from which the mean diameter of the Pt NPs could be estimated. It was found that Pt NPs with a quasi-uniform size and narrow size distribution were evenly deposited on the exterior surface of the CNTs in all the cases with a Pt loading of ≤50 wt%. As we further increased the Pt loading density up to a level of 72.1 wt%, the TEM observations (Fig. 1e) showed that all nanotube exterior surfaces were densely wrapped in Pt NP layers.

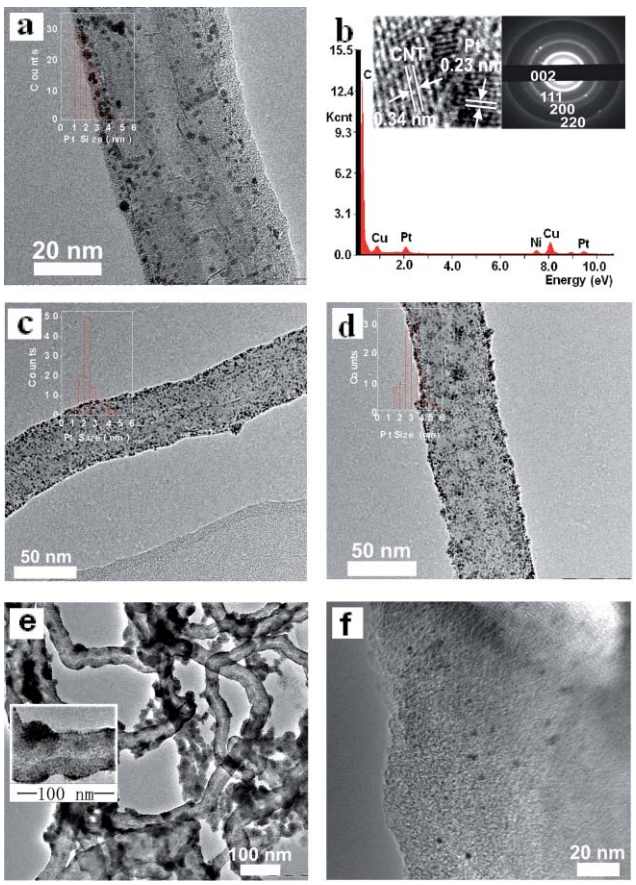

Fig. 1 (a) TEM observation for the catalyst at 10 wt% Pt loading with a diameter distribution histogram of the Pt NPs being shown in the inset. (b) Energy dispersive X-ray spectroscopy (EDS) analysis performed during the TEM observation; the left and right insets correspond to a high-resolution TEM image and the SAED pattern of the catalyst denoted in (a), respectively. (c) TEM observation for the catalyst at 27.4 wt% Pt loading with the diameter distribution histogram of the Pt NPs being shown in the inset. (d) TEM observation for the catalyst at 50 wt% Pt loading with the diameter distribution histogram of the Pt NPs being shown in the inset. (e) TEM observation for the catalyst at 72.1 wt% Pt loading. (f) TEM observation for 5 wt% Pt/C commercially obtained from Alfa Aesa.

The presence of Pt was confirmed by *in situ* energy dispersive X-ray spectroscopy (EDS) analysis, performed during the TEM observation (Fig. 1b). The selected-area electron diffraction (SAED) pattern for the catalyst consisted of several resolved concentric rings (right inset of Fig. 1b), attributable to the {111}, {200} and {220} crystal planes of face-centered cubic (fcc) Pt, as well as the {002} reflection of a hexagonal graphite structure.[16] High-resolution TEM measurements (left inset of Fig. 1b) further indicated the high crystallinity of the NPs, with an interplanar spacing of 0.23 nm corresponding to the {111} facet of Pt(0), as well as a clear layer separation of 0.34 nm attributed to the MWNTs.[16]

From the TEM observations, it is clear that the sizes of the Pt particles increase with the Pt loading content (see Fig. 2a) and that the Pt NP size can be tuned in the range 1.9 to 3.5 nm by simply manipulating the Pt loading from 1.0 to 60.6 wt%. In addition, the size of the Pt NPs was still very small (*e.g.*, around 3.5 nm) and uniform, even as the Pt loading was increased to the high level of 60.6 wt%. We plotted the Pt particle size as a function of the cubic root of the Pt/MWNT mass ratio, taken as α, as presented in Fig. 2b. Note that the particle size remains constant within error variation, regardless of the increase of $\alpha^{1/3}$ below $\alpha^{1/3} = 0.46$ (*i.e.* $\alpha \leq 0.1$). This is probably caused by the fact that more suitable defects on the nanotube walls are available for Pt nucleus deposition at $\alpha^{1/3} \leq 0.46$. However, the particle size dependently increases with the rise of $\alpha^{1/3}$ at $\alpha^{1/3} > 0.46$. In a simple sphere model, the number of Pt NPs attached onto CNTs can be expressed as $6\alpha m_{CNT}/(\pi\rho_{Pt}D^3)$, where ρ_{Pt} is the Pt density (taken to be 21.4 g cm^{-3}), m_{CNT} is the nanotube mass and D is the Pt nanoparticle diameter. The dashed line in Fig. 2b is the fit to this data at $\alpha^{1/3} > 0.46$, which suggests that the particle size is approximately in a linear relation with $\alpha^{1/3}$. This implies that the number of Pt NPs remains unchanged at $\alpha^{1/3} > 0.46$, even when the Pt loading attains a higher value. This is reasonable, provided there is a favorable deposition of Pt NPs on the defects of the nanotube walls, and there are fixed defects and curvature behaviors of the nanotubes, induced probably by tip sonication over equal timescales. The fit line gives a value of 2.9×10^{18} Pt NPs per gram of MWNTs, which also indicates the absorption sites of the nanotubes. Moreover, we estimated the number of individual MWNTs, using

$$m_{CNT}/(\rho_{CNT}V_{CNT}) = 4m_{CNT}/\pi\langle D_{CNT}\rangle 2L_{CNT},$$

where m_{CNT} is the bulk mass of the nanotubes, ρ_{CNT} is the nanotube density (1500 kg m^{-3}), V_{CNT} is the volume of an individual nanotube, D_{CNT} and L_{CNT} correspond to the diameter and length of the nanotubes, respectively. In view of both this equation and the value of 2.9×10^{18} Pt NPs per gram of MWNTs,

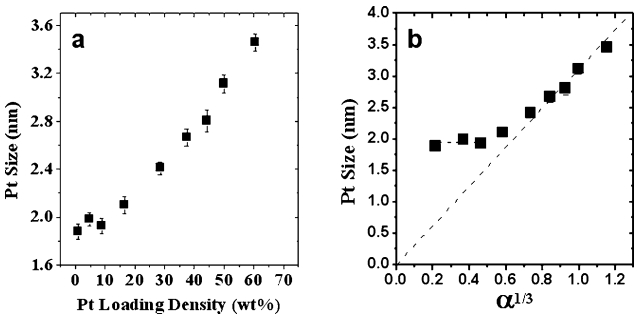

Fig. 2 Particle size as a function of (a) the Pt loading density and (b) the cube root of the Pt/MWNT mass ratio.

we could work out the number of Pt NPs per MWNT to be 42 706 by

$$(2.9 \times 10^{18})(\pi \langle D_{CNT} \rangle 2L_{CNT})/(4 \times 10^{-3}),$$

where D_{CNT} and L_{CNT} are taken to be 50 nm and 5 μm, respectively.

To explore the oxidation states of the various species in the as-prepared Pt/MWNT catalysts, the Pt/MWNT composites were examined by X-ray photoelectron spectroscopy (XPS). The wide survey profile of XPS for the catalyst of 5 wt% Pt loading (Fig. 3a) showed pronounced Pt peaks, in addition to the peak of C originating from the MWNT support and background. The minor amount of oxygen probably arises from absorbed oxygen species and/or the oxygen-containing functional groups present in the raw MWNTs. No trace of other heteroelements, including Cl, was detectable, ruling out the presence of unreacted precursor or the formation of by-products in the system. The Pt 4f core level XPS pattern (Fig. 3b) fitted with the expected 4 : 3 peak area ratio, and the 3.3 eV peak separation showed asymmetric peaks with a doublet structure, *i.e.* the Pt $4f_{7/2}$ and $4f_{5/2}$ binding energy (BE) centered at 72.5 and 75.8 eV, respectively. The Pt/MWNT catalysts with Pt loadings of 10 and 27.4 wt% displayed similar XPS spectra, where the Pt $4f_{7/2}$ BEs were centered at 72.0 and 71.9 eV, respectively. The Pt NPs in the catalysts can be ascribed to Pt(0), since they were produced through the reduction of H_2PtCl_4 with excessive $NaBH_4$. However, the Pt $4f_{7/2}$ BEs of the Pt/MWNT catalyst shifted remarkably to higher values compared to the BE of Pt foil (Pt $4f_{7/2} = 70.7$ eV). This shift is probably attributable to the small size of the Pt NPs,[17] and the strong interaction between them and the CNT support.[18] For comparison, we also made an XPS measurement of the commercial 5 wt% Pt/C catalyst and found that the Pt $4f_{7/2}$ BE in this catalyst was centered at 71.8 eV (Fig. 3c). This value is lower than that of the 5 wt% Pt/MWNT catalyst, though the sizes of Pt NPs in these two catalysts were approximately identical (the sizes of the Pt NPs in 5 wt% Pt/C can be estimated from TEM measurements, as shown in Fig. 1f). Thus, the larger shift in Pt BE (≈1.8 eV) for the 5 wt% Pt/MWNT catalyst may be mainly due to the stronger interaction between the Pt and the CNT support, probably originating from charge transfer from Pt to the CNT surface. The alteration in the electronic structure of the Pt particles probably leads to the enhancement in the catalytic properties of the Pt/MWNT catalyst compared to the Pt/C catalyst. The other two weaker doublets in the Pt 4f core level XPS pattern (shown in Fig. 3b) indicate the presence of a small amount of Pt oxides, which may result from the slight oxidation of the Pt NPs upon exposure of the products to ambient air.

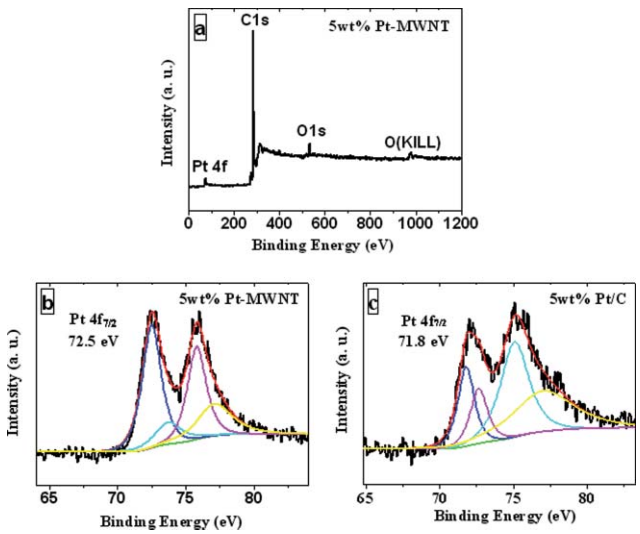

Fig. 3 (a) The wide survey XPS spectrum and (b) Pt 4f core level XPS pattern of the as-prepared 5 wt% Pt/MWNT catalyst. (c) The Pt 4f core level XPS pattern of commercial 5 wt% Pt/C.

The as-prepared Pt/MWNT catalysts, with varying Pt loadings, were used to catalyze NB hydrogenation under solvent-free conditions; the results are listed in Table 1. Note that our catalysts are indeed very catalytically active for NB hydrogenation with good selectivity to aniline. For the reaction carried out at 333 K and a H_2 pressure of 4.0 MPa, the Pt/MWNT catalyst with a 5 wt% Pt loading achieved 100% conversion of NB within 7 min with a selectivity of 100% towards aniline (entry 1). In this case, the turnover frequency (TOF) with respect to NB conversion reached 66 900 h^{-1}. As far as we are aware, this is the first report concerning NB hydrogenation with such a high performance. Although lowering the reaction temperature led to a decrease in the TOF (entries 1 and 4), the TOF value of the reaction conducted at 308 K and a H_2 pressure of 4 MPa was

Table 1 Catalytic results of nitrobenzene hydrogenation over the as-prepared Pt/MWNT catalysts

		Reaction conditions					
Entry	Catalyst	T/K	P_{H_2}/MPa	Time/min	Conversion (%)	AN selectivity (%)	TOF/h[a]
1	5 wt% Pt/MWNT[b]	333	4	7	100	100	66 900
2	5 wt% Pt/MWNT[b]	333	2	9	99.9	99.8	52 000
3	5wt% Pt/MWNT[b]	333	0.6	23	99.9	99.9	20 300
4	5 wt% Pt/MWNT[b]	308	4	12	98.6	99.3	38 400
5	5 wt% Pt/MWNT[b]	308	2	19	97.7	99.3	24 000
6	27.4 wt%Pt/MWNT[c]	333	2	10	100	99.7	17 100
7	50 wt% Pt/MWNT[d]	333	2	12	99.8	99.8	14 200
8	27.4 wt% Pt/MWNT[e]	333	2	108	99.9	99.8	15 800
9	10 wt% Pt/C[c]	333	2	34	98.2	98.0	13 500
10	5 wt% Pt/C[b]	333	2	9	42.9	94.8	22 300

[a] TOF of NB conversion (mol NB converted per mol Pt per h). [b] Substrate (0.01 mol), 5 mg catalyst (0.25 mg Pt). [c] Substrate (0.01 mol), 2.5 mg catalyst (0.685 mg Pt). [d] Substrate (0.01 mol), 1.4 mg catalyst (0.7 mg Pt). [e] Substrate (0.1 mol), 2.5 mg catalyst (0.685 mg Pt).

still as high as 38 400 h^{-1} at an NB conversion of 98.6% with a 99.3% selectivity to aniline (entry 4). This outweighs the best results reported so far for this reaction.[19] From Table 1, it also can be observed that the TOF can attain a very high value, even at a low pressure (*e.g.*, 0.6 MPa, entry 3), despite the fact that reducing the H_2 pressure considerably results in a corresponding decline in the TOF (entries 1–3).

The increase of Pt content from 5 to 27.4 to 50 wt% in the Pt/MWNT catalysts unambiguously gives rise to the decrease in the corresponding TOF (entries 2, 6, 7), which is most likely attributable to the increased Pt NP size with increasing Pt loading.[20] To study if the catalytic hydrogenation is structure sensitive, we explored the overall reaction rates of NB conversion per exposed Pt surface atom as a function of NP size. The fraction of active Pt surface atoms can be calculated by A/d_{Pt}, where A is a constant dependant on the catalyst species and d_{Pt} is the volume-area mean particle diameter.[21] In such scenarios, the reaction rate of NB conversion normalized to the exposed metal surface atoms can be given by

$$[(d_{Pt}\ \langle TOF\rangle)/A]\ (h^{-1}).$$

If we assume that d_{Pt} is equal to the Pt crystallite size, estimated by TEM measurements, the reaction rate is found to decrease remarkably, albeit with a slight increase in NP size from 2.0 to 2.4 nm as the Pt content is increased from 5 to 27.4 wt%, *i.e.*

$$[(d_{Pt}\ \langle TOF\rangle)/A]_{5\ wt\%\ Pt/MWNT} = 104\,000/A,$$

$$[(d_{Pt}\ \langle TOF\rangle)/A]_{27.4\ wt\%\ Pt/MWNT} = 41\,040/A).$$

However, the value of the normalized reaction rate for 27.4 wt% Pt/MWNT approximates to that for 50 wt% Pt/MWNT (*i.e.*

$$[(d_{Pt}\ \langle TOF\rangle)/A]_{50\ wt\%\ Pt/MWNT} = 44\,020/A),$$

regardless of the further increase of the NP size from 2.4 to 3.1 nm. These results strongly suggest that the reaction is structure sensitive when the Pt size is within a certain range, highly probably in the range of 2–2.4 nm, beyond which the reaction behaves as structure insensitive.

We must point out that the calculated reaction rate based on the above assumption is overestimated due to an overestimation of the volume-area mean particle size as a result of the superimposition of neighbouring Pt particles at high Pt loadings. In light of this consideration, it is not surprising that the calculated reaction rate for the 50 wt% Pt/MWNT is slightly higher than that for the 27.4 wt% Pt/MWNT. We increased the substrate/catalyst molar ratio nine-fold and obtained an analogous TOF value and good selectivity (entries 6 and 8). This suggests the availability of the as-prepared catalysts for scaling up the hydrogenation reaction. Note that the catalysts with 27.4 wt% and 50 wt% Pt loadings showed better performance than the commercial 10 wt% Pt/C catalyst (entries 6, 7 and 9). This is of utmost importance for practical applications, where higher metal loadings are required without a serious loss of catalytic performance.

Despite the large volume of work available with respect to the hydrogenation of NB, very few reports have highlighted the reaction mechanism. The first model was proposed by Haber in 1898, which involves two reaction pathways: the direct route and the condensation route.[22] Following this scheme, several related mechanisms have been proposed based on the identification of reaction intermediates over various catalysts.[23–25] To explore the reaction pathway of NB hydrogenation over the Pt/MWNT catalysts, we tracked the yields of the different products as a function of reaction time. Fig. 4 displays the reaction profile of NB hydrogenation over the Pt/MWNT catalyst with a 5 wt% Pt loading. It was found that NSB and AOB, both with yields less than 3%, were the only two intermediates, and no other intermediates accumulated in measurable amounts during the process of NB conversion. This differs from previously reported studies, which unambiguously showed the occurrence of PHA accumulation during the hydrogenation process.[23–25] As a result of this finding, it can be deduced that the reported schemes, so far, do not seem to be fully valid here for our Pt/MWNT catalyst.

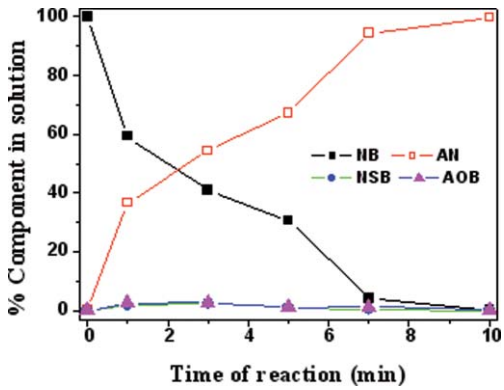

Fig. 4 Reaction profile of NB hydrogenation over Pt/MWNT with 5 wt% Pt.

As NSB and AOB were detected during the reaction's progress, one possibility for aniline production may lie in the combination of the direct transformation of NSB to aniline and the condensation of NSB to AOB, followed by its further conversion to aniline. To check this possibility, we used NSB as a reactant and performed the hydrogenation of NSB in aniline using the Pt/MWNT catalyst under otherwise identical conditions to those used for the NB hydrogenation. The results showed that NSB converted to AOB in >95% yield and that no PHA was detectable within the same reaction time, consistent with the results presented by Gelder *et al.*[24] and Corma *et al.*[25] As the reaction time was further prolonged, aniline was formed. This indicates that the condensation of NSB to AOB, and further to aniline, is the main reaction pathway for aniline production by NSB hydrogenation. Moreover, it can be deduced that the rate of aniline production from NSB hydrogenation is much lower than that from NB hydrogenation. All of these observations justify the conclusion that the route from NSB to aniline made a less important contribution to the production of aniline during the NB hydrogenation. On the basis of our experimental results and discussion, we propose a new reaction pathway for NB hydrogenation over our Pt/MWNT catalyst, in which aniline is produced predominantly through the very rapid hydrogenation of NB without detectable PHA accumulation, and that a small proportion of the aniline results from a sequential transformation: NB→NSB→AOB→AN. The specific reaction pathway may be highly attributed to the remarkable catalytic

performance of the Pt/MWNT catalyst, probably resulting from the special interaction between the MWNTs and the Pt NPs, as evidenced by the large shift of the Pt $4f_{7/2}$ BE.

Conclusion

In summary, ultrafine Pt NPs have been uniformly deposited onto nanotube surfaces *via* a very simple sonication process. The particle size can be controllably tuned in the range 1.9–3.5 nm by manipulating the weight ratio of the precursor to the nanotubes. It is worth noting that the sizes of the Pt particles on the CNTs are surprisingly small ($\leq$3.5 nm), even at very high Pt loadings (*i.e.* 50 wt%). The as-prepared Pt/MWNT catalysts have unprecedented activity and selectivity for the hydrogenation of NB to aniline in the absence of solvent under mild conditions. It has been demonstrated that aniline is formed predominately from the very rapid hydrogenation of NB, without PHA accumulation. This catalyst makes the process interesting from both an economic and an environmental point of view, and thus could potentially be applied to the catalytic green hydrogenation of NB.

Experimental

Materials

All chemicals used in this work were of analytical grade and used as supplied. Multi-walled carbon nanotubes (MWNTs) were purchased from Shenzhen Nanotech Port Co., Ltd. and used without further treatment. The outer diameters and lengths of the MWNTs were 40–60 nm and 1–12 μm, respectively. 5 wt% Pt/C (lot code: 10123314) and 10 wt% Pt/C (lot code: 1392349) catalysts were commercially obtained from Alfa Aesa and Aldrich, respectively.

Synthesis of Pt/MWNT catalysts

In a typical experiment, 10 mg of MWNTs were initially dispersed in 20 mL of a $H_2PtCl_6{\cdot}6H_2O$ ethanol solution at a designated concentration to form a uniform suspension *via* tip sonication (500 W, 20 kHz, 20% amplitude power output) for 4 min. Then, 1 mL of a $NaBH_4$ ethanol solution (its concentration being 3 times higher than that of the precursor used) was dropped into the suspension under tip sonication within 2 min. Subsequently, the obtained sample was ultracentrifuged, the collected precipitate washed repeatedly with absolute ethanol and distilled water, and then vacuum dried at 60 °C for 6 h. The loading density of Pt on the MWNTs could be easily tuned by altering the weight ratio of the precursor to the nanotubes.

The hydrogenation of nitrobenzene (NB) and nitrosobenzene (NSB)

The same catalyst testing procedure was followed for each run. Typically, the desired amount of catalyst (Pt/MWNT) and NB or NSB dissolved in aniline were loaded into a high pressure stainless steel reactor; the reactor was then sealed and flushed with H_2 three times to remove the air inside. Subsequently, the reactor was moved to a water bath set at a desired temperature and H_2 introduced up to the required pressure. The hydrogenation reaction was carried out with magnetic stirring (625 rpm). The H_2 pressure was kept constant by replenishing the H_2 as the reaction proceeded. The resultant sample, after removing the catalyst and the water produced by ultracentrifugation, was analyzed by gas chromatograph (Agilent 4890D) using a capillary column.

Acknowledgements

This work was financially supported by the National Natural Science Foundation of China (no. 20903105) and the Chinese Academy of Sciences (KJCX2.YW.H16).

References

1 A. S. Travis, in *The Chemistry of Functional Groups: The Chemistry of Anilines*, ed. Z. Rappoport, Wiley-VCH, Weinheim, 2007, pp. 715–782.
2 *Handbook of Heterogeneous Catalytic Hydrogenation for Organic Synthesis*, ed. S. Nishimura, Wiley-VCH, Weinheim, 2001, pp. 332.
3 H. Li, Q. Zhao, Y. Wan, W. Dai and M. Qiao, *J. Catal.*, 2006, **244**, 251–254.
4 F. Figueras and B. Coq, *J. Mol. Catal. A: Chem.*, 2001, **173**, 223–230.
5 F. Y. Zhao, Y. Ikushima and M. Arai, *J. Catal.*, 2004, **224**, 479–483.
6 I. M. J. Vilella, S. R. de Miguel and O. A. Scelza, *Chem. Eng. J.*, 2005, **114**, 33–38.
7 J. W. G. Wilder, L. C. Venema, A. G. Rinzier, R. E. Smalley and C. Dekker, *Nature*, 1998, **391**, 59–62.
8 T. W. Odom, J. L. Huang, P. Kim and C. M. Lieber, *Nature*, 1998, **391**, 62–64.
9 M. J. O'Connell, S. M. Bachilo, C. B. Huffman, V. C. Moore, M. S. Strano, E. H. Haroz, K. L. Rialon, P. J. Boul, W. H. Noon, C. Kittrell, J. Ma, R. H. Hauge, R. B. Weisman and R. E. Smalley, *Science*, 2002, **297**, 593–596.
10 M. Fujiwara, E. Oki, M. Hamada, Y. Tanimoto, I. Mukouda and Y. Shimomura, *J. Phys. Chem. A*, 2001, **105**, 4383–4386.
11 T. W. Ebbesen, H. J. Lezec, H. Hiura, J. W. Bennett, H. F. Ghaemi and T. Thio, *Nature*, 1996, **382**, 54–56.
12 R. H. Baughman, A. A. Zakhidov and W. A. de Heer, *Science*, 2002, **297**, 787–792.
13 M. M. J. Treacy, T. W. Ebbesen and J. M. Gibson, *Nature*, 1996, **381**, 678–680.
14 Y. Lin, X. Cui, C. Yen and C. M. Wai, *J. Phys. Chem. B*, 2005, **109**, 14410–14415.
15 Y. Xing, *J. Phys. Chem. B*, 2004, **108**, 19255–19259.
16 J. Y. Chen, T. Herricks, M. Geissler and Y. N. Xia, *J. Am. Chem. Soc.*, 2004, **126**, 10854–10855.
17 W. Eberhardt and P. Fayet, *Phys. Rev. Lett.*, 1990, **64**, 780–784.
18 C. Bittencourt, M. Hecq, A. Felten, J. J. Pireaux, J. Ghijsen, M. P. Felicissimo, P. Rudolf, W. Drube, X. Ke and G. Van Tendeloo, *Chem. Phys. Lett.*, 2008, **462**, 260–264.
19 X. C. Meng, H. Y. Cheng, Y. Akiyama, Y. F. Hao, W. B. Qiao, Y. C. Yu, F. Y. Zhao, S. Fujita and M. Arai, *J. Catal.*, 2009, **264**, 1–10.
20 E. A. Gelder, S. D. Jackson and C. M. Lok, *Catal. Lett.*, 2002, **84**, 205–208.
21 N. Mahata and V. Vishwanathan, *J. Catal.*, 2000, **196**, 262–270.
22 F. Haber, *Z. Elektrochem.*, 1898, **22**, 506–514.
23 I. A. Makaryan and V. I. Savchenko, *Stud.Surf. Sci. Catal.*, 1993, **75**, 2439–2442.
24 E. A. Gelder, S. D. Jackson and C. M. Lok, *Chem. Commun.*, 2005, 522–524.
25 A. Corma, P. Concepción and P. Serna, *Angew. Chem., Int. Ed.*, 2007, **46**, 7266–7269.